This article has been accepted for publication in a future issue of this journal, but has not been fully edited. Content may change prior to final publication. Citation information: DOI 10.1109/TSG.2016.2609603, IEEE Transactions on Smart Grid

Enhancing Resilience of Microgrids with Electric Springs

Liang Liang, *Student Member, IEEE*, Yunhe Hou, *Senior Member, IEEE*, David. J. Hill, *Life Fellow, IEEE*, and S. Y. Ron Hui, *Fellow, IEEE*

***Abstract*—Extreme natural events have caused severe power system blackouts in recent years. It is important for power systems to survive after such events and recover the power supply, especially for critical loads (CLs), as soon as possible. In this paper, a control strategy is proposed for electric springs (ESs) to enhance resilience of microgrids with fluctuating renewable resources. First, the feasible operating region of the ES and the power-voltage curve of the bus connected with the ES are derived analytically. Second, according to the derived feasible operating region, a novel control strategy of ES is proposed to regulate the frequency and voltage of microgrids with and without a communication system. The voltages on CLs are considered as a critical constraint for enhancing resilience during extreme natural events. Finally, the method to enhance resilience of microgrids with ES under both the frequency support mode and the voltage support mode are studied. Case studies demonstrate that ESs can enhance the resilience of microgrids with the proposed strategy with and without a communication system after extreme natural events.**

***Index Terms*—Electric spring, microgrid, renewable energy, resilience.**

NOMENCLATURE

B_{ij}	Susceptance of the branch between bus *i* and *j*.
D	Parameter of load frequency characteristic.
f_d^-, f_d^+	Negative and positive threshold of the dead band of frequency deviation.
f_{min}, f_{max}	Minimum and maximum frequency deviations.
G_{ij}	Conductance of the branch between bus *i* and *j*.
I_k^{NCL}	Branch current of non-critical load (NCL) at bus k.
M	Parameter of load frequency characteristic.
NB	Number of bus nodes.
P_i^D, Q_i^D	Active and reactive power of load at bus *i*.
$P_k^{D,max}$	Maximum consumed power by bus *k* in the feasible region of x_k.
$P_k^{D,min}$	Minimum consumed power by bus *k* in the feasible region of x_k.
P_i^G, Q_i^G	Active and reactive power output of generator at bus *i*.
$P_k^{BUS,max}, P_k^{BUS,min}$	Maximum and minimum consumed active power for the bus *k* with ES.
P_k^{init}	Initial consumed power of bus *k* installed with electric spring (ES).
P_k^{CL}	Active power on the critical load (CL) at bus *k*.
P_k^{NCL}	Active power on the NCL at bus *k*.
$P_{k,max}^{NCL}$	Maximum consumed active power by the NCL at bus *k*.
R_k^{NCL}	Resistance of the NCL at bus *k*.
S_{Diesel}	Rated apparent power of the diesel generator.
V_k	Voltage at bus *k*.
V_k^{max}, V_k^{min}	Upper and lower boundaries of acceptable voltage region.
V_k^{ES}	Output voltage of the ES at bus *k*.
$V_k^{ES,\text{Set}}$	Set point of ES output voltage.
$V_k^{BUS,max}, V_k^{BUS,min}$	Maximum and minimum voltage for the bus *k* with ES.
V_k^{NCL}	Voltage on the NCL at bus *k*.
x_k	Represents the V_k^{ES}/V_k on bus *k*.
x_k^{min}, x_k^{max}	*x* for the minimum and maximum consumed active power on the NCL.
x_k^{init}	Value of *x* for the frequency deviations within the dead band.
X_k^{NCL}	Reactance of the NCL at bus *k*.
Z_k^{CL}	Impedance of the CL at bus *k*.
Z_k^{NCL}	Impedance of the NCL at bus *k*.
γ_k	Ratio between the voltage on the NCL and the bus *k*.
φ_k^{NE}	Angle between the voltage vector of ES output and the voltage vector of NCL.
φ_k^{NCL}	Power angle of the NCL at bus *k*.
χ_{dec}	Set of x_k, where γ_k is a decreasing function of x_k.
χ_{inc}	Set of x_k, where γ_k is an increasing function of x_k.

This work was fully supported by the Research Grants Council of the Hong Kong Special Administrative Region under the Theme-based Research Scheme through Project No. T23-701/14-N, National Natural Science Foundation of China (51277155), National Key Research Program (973 Program, 2012CB215102), Research Grant Council, Hong Kong SAR (ECS739713 and GRF 17202714), and Basic Research Program-Shenzhen Fund (JCYJ20150629151046877).

L. Liang and Y. H. Hou are with the Department of Electrical and Electronics, the University of Hong Kong, Hong Kong SAR, China and Shenzhen Institute of Research and Innovation, the University of Hong Kong, Shenzhen, China. D. J. Hill, and S. Y. R. Hui are with the Department of Electrical and Electronics, the University of Hong Kong, Hong Kong SAR, China (e-mails: lliang@eee.hku.hk, yhhou@eee.hku.hk, dhill@eee.hku.hk, and ronhui@eee.hku.hk).

I. INTRODUCTION

EXTREME natural events in recent years have caused immense losses to power systems and societies. Recent severe power outages caused by extreme natural events such as Superstorm Sandy [1], are powerful reminders that energy infrastructure resilience requires significant enhancement. Resilience is defined as "The ability to prepare for and adapt to changing conditions and withstand and recover rapidly from disruptions" [2]. In power systems, the North American Electric Reliability Corporation (NERC) and the United States Electric Power Research Institute (EPRI) have been actively developing innovative technologies aimed at enhancing resilience. Although the functionary requirements of resilience are very diverse, the ability to adapt unfolding extreme natural events and to restore from an outage are identified. Especially, the survivability of critical loads during extreme natural events has been widely highlighted [2].

To meet the requirements of system resilience, it appears that microgrids play important roles, especially for distribution systems [3-5]. As a critical function of resilience, after an extreme natural events, microgrids in islanded mode or grid-connected mode, are expected to restore the system as quickly as possible. Especially, it is important to restore critical loads (CLs). However, it is a challenging task for microgrids to maintain system frequency and bus voltages with limited operating resources and small system inertia, especially, after a major outage. The frequency deviations should be kept within operating limits in order to avoid permanent damage to the diesel and steam generators. Some CLs are sensitive to the power quality. The voltage deviations at the CLs should be reduced in order to guarantee a reliable supply at CLs.

Sufficient operating resources are essential for the resilience of microgrids. Researchers have proposed various methods to enhance to controllability with limited operating resources from all components of systems. As proposed in [6], power converter based wind energy generation systems can be operated to increase the system inertia by implementing frequency droop control. An identical control strategy has been applied on several different kinds of renewable generation systems and energy storage systems to increase the system inertias as proposed in [7-9]. However, it is still a challenging task for microgrids to reliably supply the CLs in microgrids with fluctuating renewable energy after extreme natural events. Recently, loads have also been proposed as a type of operating resource by implementing load-response [10]. As described in [11], load-response can contribute to the frequency control. With the development of technology, load responses have been identified as one of the critical resources to enhance system resilience.

According to operating characteristics of loads, some techniques have been developed to make the loads more flexible and contribute further to the power system operation. Electric spring (ES) has been well identified as a state-of-the-art technology to implement load response [12]. Comparing with the other existed technologies to improve the power quality as shown in Table I, an ES can improve the voltage quality of the CLs by passing fluctuations of renewable energy to the non-critical loads (NCLs) [13, 14]. The output voltage of an ES is perpendicular to the current vector of the NCL. This operating principle is similar to a static synchronous series compensator (SSSC) listed in Table I. Different from the operating methods of dynamic voltage restorer (DVR) and static synchronous compensator (STATCOM), an ES is installed on the NCL while a DVR or a STATCOM is installed on the CL to improve the power quality of the CL. As described in [15], an ES may achieve a more efficient result than a STATCOM for regulating bus voltage under some cases. An ES can also participate in frequency regulation by controlling the active power on the NCLs and implement a primary frequency control [16]. Until now, the proposed method is mainly focused on determining the active power on an NCL and the bus voltage variations. Few, if any work address the active power on the CLs and the method for setting the initial operating point of ES. To enhance resilience of a microgrid with load response associated with ES, the operating limits of ES should be well identified and control strategies should be designed according to these limits.

The major contributions of this paper are outlined as follows:

1) To enhance the resilience of a microgrid with ES, the feasible operating region of ES output voltage and the power-voltage curves of the bus connected with the ES are derived analytically. Within the feasible operating region, the DC link voltage of the ES can be maintained as a constant so that the ES can be operated continuously without energy storage devices.

2) A novel control strategy is proposed for the ES in microgrids to facilitate the supply of CLs with both frequency control and voltage control. An optimization model is designed for the proposed control strategy in order to determine the operating limits of the ES and the initial operating points, considering the voltage constraints on CLs.

3) The proposed strategy of the ES is employed to enhance the resilience of microgrids by facilitating frequency and voltage control.

TABLE I
COMPARISON OF ES WITH OTHER TECHNOLOGIES

Name	Topology	Operating Methods & Targets
ES	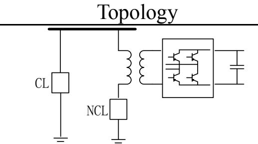	Regulate bus voltage by adjusting output voltage vector, which is perpendicular to current vector of the NCL
SSSC	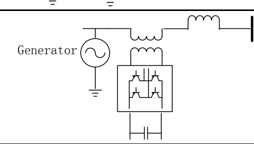	Compensate reactance of transmission line by inserting a voltage vector, which is perpendicular to current vector
DVR	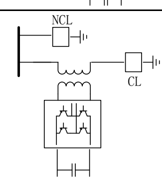	Regulate the voltage on CL by inserting a voltage vector, which equals to the difference between bus voltage and nominal voltage
STATCOM	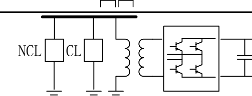	Regulate bus voltage by inserting reactive current

The rest of this paper is organized as follows. The concept of resilience of microgrids and the analysis of feasible operating region of an ES are explained in Section II. The proposed local control of the ES is described in Section III, followed by the optimization model of the ES in Section IV. The case studies and the discussions are presented in Section V and finally, the conclusions are drawn in Section VI.

II. THE RESILIENCE OF MICROGRIDS WITH ES

A. The Resilience of Microgrids

As indicated in [2], microgrids can contribute to system resilience by their flexible operating strategies. One of operating scenarios is that several microgrids are connected with each other by a distribution network as shown in Fig. 1. The CLs are distributed within some microgrids and installed with the ESs. After extreme natural events, the distribution networks may not be able to connect with the bulk power system. How to maintain reliable supply of the CLs after extreme natural events is one of the major concern of the resilience of microgrids [1]. CLs can be restored by their own microgrids or other microgrids. Some microgrids may able to restore with their own operating resources so that the CLs in

This article has been accepted for publication in a future issue of this journal, but has not been fully edited. Content may change prior to final publication. Citation information: DOI 10.1109/TSG.2016.2609603, IEEE Transactions on Smart Grid

these microgrids can be restored quickly. However, some microgrids may not be restored owing to part or entire loss of their operating resources and the CLs in them cannot be supplied. In order to power these CLs, one or more restored microgrids can restore the CLs through available connections in the distributed network. The key technical requirement for implementing this critical functionary requirements is the microgrids should have the capability to maintain frequency and voltage levels of CLs.

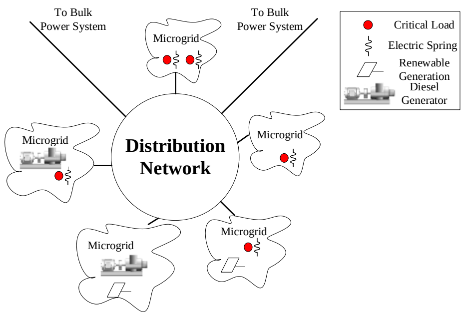

Fig. 1. Structure of a distribution network based on microgrids.

In order to supply the CLs reliably, the system frequency and bus voltage should be controlled within acceptable regions. Owing to smaller system inertia and operating resources when the microgrid is disconnected from the bulk power system, this is a challenging. ES provide an alternative method to implement this function. In this paper, in addition to the original voltage support mode of an ES, a frequency support mode is proposed to support the frequency of islanded microgrids. The NCLs in the microgrids are treated as operating resources by the ESs in order to regulate the system frequency and voltage on the CLs. With the proposed strategies, ESs can be operated coordinately if the communication system is functional after the extreme natural events or individually with their local information. Under different modes of ES, CLs can be reliably powered during the restoration process. As a result, resilience of the system can be enhanced.

B. Feasible Operating Region of an ES

To implement the functionary of resilience, ESs and CLs may be configured as in [14]. An ES is connected in series between the bus and the NCL. A CL is connected directly to the bus and operated in parallel with the NCL and the ES branch. The bus voltage and the voltage on the NCL can be adjusted by controlling the output voltage vector of the ES. The NCL and the CL are modeled by combinations of different kinds of passive elements, such as resistors, reactors, and inductors. The active and reactive power of both the NCL and the CL are associated with the bus voltage and the voltage on CL is needed to be controlled within a secured region in order to make sure that the CL is supplied properly.

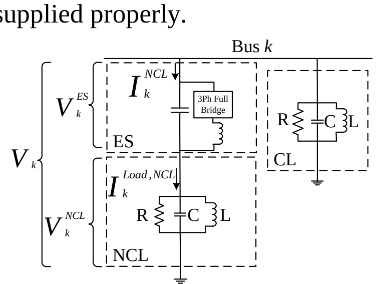

(a) Hardware of an electric spring

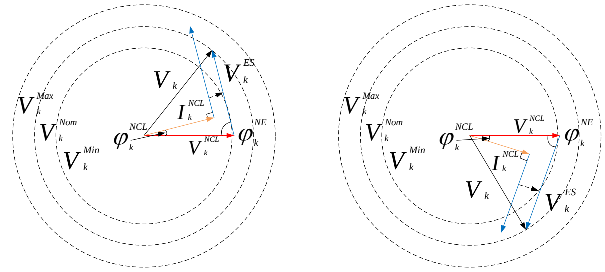

(b) Inductive mode (c) Capacitive mode

Fig. 2. Voltage and current vectors of an ES under two operation modes.

As shown in Fig. 2, the output voltage of an ES is perpendicular to the current vector of the NCL so that energy storage elements, such as batteries, are not needed to maintain the continuous operation of ES [17]. The power loss during the operation of an ES can be compensated via dc voltage control as in [18] and the compensation actions will add a small angle deviation between the ES output voltage vector and the current vector of the NCL. Considering the relatively small value of power loss of an ES operation and the good performance of a phase lock loop (PLL) to trace the angle deviation caused by the power loss, the power loss is neglected in this paper so that the ES output voltage is regarded to be perpendicular to the current vector of the NCL. The ES is operated under inductive and capacitive modes as shown in Fig. 2(b) and Fig. 2(c) for leading and lagging power factors of the NCL. The φ_k^{NCL} represents the power angle of the NCL and it is defined as positive for the NCL with a leading power factor and negative for the NCL with a lagging power factor. The relationship among the vectors in Fig. 2 can be described by the following equations,

$$V_k{}^2 = V_k^{NCL^2} + V_k^{ES^2} - 2V_k^{NCL}V_k^{ES}\cos\varphi_k^{NE} \quad (1)$$

$$\varphi_k^{NE} = 90^\circ \pm \varphi_k^{NCL}. \quad (2)$$

For an ES under inductive mode,

$$\varphi_k^{NCL} = \pi/2 - \varphi_k^{NE} \quad (3)$$

$$V_k{}^2 = V_k^{ES^2} + V_k^{NCL^2} - 2\sin\varphi_k^{NCL}\,V_k^{ES}V_k^{NCL}, \quad (4)$$

and for an ES under capacitive mode,

$$\varphi_k^{NCL} = \pi/2 + \varphi_k^{NE} \quad (5)$$

$$V_k{}^2 = V_k^{ES^2} + V_k^{NCL^2} + 2\sin\varphi_k^{NCL}\,V_k^{ES}V_k^{NCL}. \quad (6)$$

Both V_k and V_k^{NCL} are positive variables in (1)-(6) owing to no directions are associated with them. The sign of V_k^{ES} represents the direction of voltage vector V_k^{ES} in Fig. 2. V_k^{ES} is specified as positive under inductive mode and negative under capacitive mode. Equations (4) and (6) can be rewritten as follows for both the modes,

$$V_k^{NCL} = \sin\varphi_k^{NCL}\,V_k^{ES} \pm \sqrt{V_k{}^2 - \cos^2\varphi_k^{NCL}\,V_k^{ES^2}}. \quad (7)$$

Let $V_k^{ES} = x_k V_k$ and $\gamma_k = V_k^{NCL} V_k$; then (7) can be expressed as follows,

$$\gamma_k = \sin\varphi_k^{NCL}\,x_k \pm \sqrt{1 - \cos^2\varphi_k^{NCL}\,x_k{}^2}. \quad (8)$$

The γ should be positive so that (8) can be represented as follows and the details of derivations are described in section A in the Appendix.

$$\gamma_k = \sin\varphi_k^{NCL}\,x_k + \sqrt{1 - \cos^2\varphi_k^{NCL}\,x_k{}^2}. \quad (9)$$

Since $\gamma_k > 0$, the feasible set of x_k is $x \in \left[-\frac{1}{\cos\varphi_k^{NCL}}, 1\right]$ for $\varphi_k^{NCL} \in \left[-\frac{\pi}{2}, 0\right]$ and $x_k \in \left[-1, \frac{1}{\cos\varphi_k^{NCL}}\right]$ for $\varphi_k^{NCL} \in \left[0, \frac{\pi}{2}\right]$.

This article has been accepted for publication in a future issue of this journal, but has not been fully edited. Content may change prior to final publication. Citation information: DOI 10.1109/TSG.2016.2609603, IEEE Transactions on Smart Grid

As shown by (7) and (9), the voltage on the NCL is determined by the output voltage of ES and the bus voltage. Thus, the active power consumed by the NCL is also determined by them as follows,

$$P_k^{NCL} = \frac{{V_k}^2{\gamma_k}^2R_k^{NCL}}{{Z_k^{NCL}}^2} = \frac{{V_k}^2\left(\sin\varphi_k^{NCL}x_k+\sqrt{1-\cos^2\varphi_k^{NCL}{x_k}^2}\right)^2R_k^{NCL}}{{Z_k^{NCL}}^2}. \quad (10)$$

III. Operation Strategy for the ES

In order to enhance the resilience of microgrid with ES, a control strategy is proposed for the ES to regulate the frequency by considering the voltage constraint on the CL.

A. Typical P-V Curves of Buses with ESs

Typical power-voltage (*P-V*) curves of a bus installed with an ES for resistive and inductive loads, which are the most representative load types in power systems, are shown in Fig. 3.

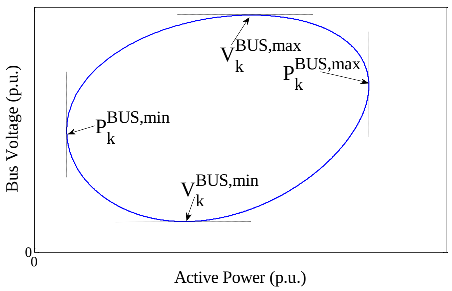

(a) $\varphi_k^{NCL} = 0$

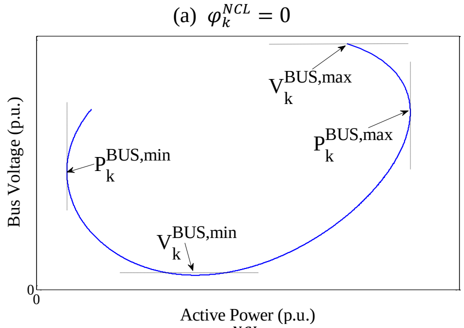

(b) $\varphi_k^{NCL} = -\pi/6$

Fig. 3. Typical power-voltage curves of the bus installed with an ES.

The *x*-axis of Fig. 3 represents the total active power consumed by bus *k*, which equals the summation of active power on the CL and the NCL. The four vertices, which are marked as $P_k^{ES,min}$, $P_k^{ES,max}$, $V_k^{ES,min}$, and $V_k^{ES,max}$, are essential parameters for the operation of an ES.

For the curve of a resistive NCL as shown in Fig. 3(a), the curve is similar to a closed ellipse. The derivations are given in section B in the Appendix. Since the feasible operating range of x_k is symmetric about zero within $[-1,1]$ for a resistive NCL, the minimum consumed active power on the NCL can be reduced to zero when x_k equals to ± 1 as in (10). However, for an inductive NCL, the feasible operating range of x_k is asymmetric about zero within $\left[-\frac{1}{\cos\varphi_k^{NCL}}, 1\right]$. The consumed active powers on the NCL are different for x_k equals to 1 and $-\frac{1}{\cos\varphi_k^{NCL}}$ as in (9) and (10). The minimum consumed active power on NCL can be reduced to zero only under x_k equals to 1. As a consequence, the curve shown in Fig. 3(b) is an unclosed arc.

B. ES with a Strong Bus and Operated Locally

If an ES is located near the controllable generators or voltage compensation devices, the bus voltage is not considerably affected by the ES. Thus, the power consumed by the CL, P_k^{CL} is also not highly affected by the ES. In this case, both the V_k and P_k^{NCL} are assumed as constants and only the power consumed by the NCL, P_k^{NCL}, is controlled by the ES in order to regulate the system frequency. The P_k^{NCL} is only determined by γ_k. The first order and the second order derivatives of $\frac{d\gamma_k}{dx_k}$ are expressed as follows,

$$\frac{d\gamma_k}{dx_k} = \sin\varphi_k^{NCL} - \frac{x_k\cos^2\varphi_k^{NCL}}{\sqrt{1-\cos^2\varphi_k^{NCL}{x_k}^2}} \quad (11)$$

$$\frac{d^2\gamma_k}{d{x_k}^2} = -\frac{\cos^2\varphi_k^{NCL}}{\sqrt{1-\cos^2\varphi_k^{NCL}{x_k}^2}} - \frac{{x_k}^2\cos^4\varphi_k^{NCL}}{\sqrt{\left(1-\cos^2\varphi_k^{NCL}{x_k}^2\right)^3}} < 0. \quad (12)$$

The set of x_k, where γ_k is an increasing function of x_k, is defined as χ_{inc} and the set of x_k, where γ_k is a decreasing function of x_k, is defined as χ_{dec}. Equation (12) indicates that P_k^{NCL} is concave with x_k. Thus, the global maximum P_k^{NCL} can be obtained by equating $\frac{d\gamma}{dx} = 0$ as follows,

$$x_k^{max} = \tan\varphi_k^{NCL}. \quad (13)$$

$$P_{k,max}^{NCL} = \frac{{V_k}^2R_k^{NCL}}{{Z_k^{NCL}}^2\cos^2\varphi_k^{NCL}} \quad (14)$$

Since P_k^{NCL} is non-negative, the minimum P_k^{NCL}, i.e. $P_{k,min}^{NCL}$, equals to zero and x_k^{min} can be solved as follows and the details of derivations are stated in section C in the Appendix.

$$x_k^{min} = \begin{cases} 1 & \varphi_k^{NCL} \in \left[-\frac{\pi}{2}, 0\right) \\ -1 & \varphi_k^{NCL} \in \left(0, \frac{\pi}{2}\right] \\ \pm 1 & \varphi_k^{NCL} = 0 \end{cases} \quad (15)$$

Based on (13) to (15), the operation range of the active power consumed by the NCL connected with an ES can be determined analytically with local information. Differently to the primary frequency control proposed in [16], a controller is proposed to control x_k that is proportional to the frequency deviations in order to regulate the system frequency for the islanded microgrid under the frequency support mode as shown in Fig. 4.

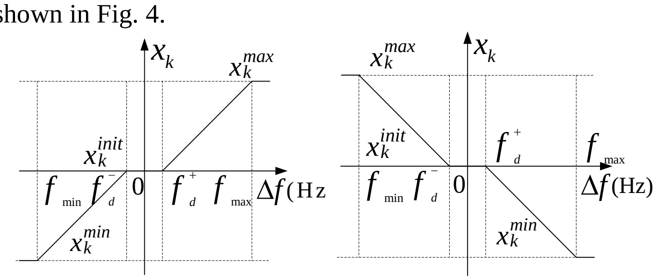

(a) $x \in \chi_{inc}$ (b) $x \in \chi_{dec}$

Fig. 4. Relationship between x_k and Δf.

As shown in Fig. 4, the x_k is proportional to the frequency deviations. A dead band is inserted to avoid the excessive control actions of multiple ESs for small frequency deviations. The control strategy in Fig. 4 can be represented as follows,

This article has been accepted for publication in a future issue of this journal, but has not been fully edited. Content may change prior to final publication. Citation information: DOI 10.1109/TSG.2016.2609603, IEEE Transactions on Smart Grid

$$x_k = \begin{cases} x_k^{max} & \Delta f > f_{max} \\ x_k^{init} + \left(x_k^{max} - x_k^{init}\right)\frac{\Delta f - f_d^+}{f_{max} - f_d^+} & f_d^+ < \Delta f \le f_{max} \\ x_k^{init} & f_d^- \le \Delta f \le f_d^+ \quad x_k \in \chi_{inc} \\ x_k^{init} - \left(x_k^{init} - x_k^{min}\right)\frac{\Delta f - f_d^-}{f_{min} - f_d^-} & f_{min} \le \Delta f < \Delta f_d^- \\ x_k^{min} & \Delta f < f_{min} \end{cases} \quad (16)$$

$$x_k = \begin{cases} x_k^{min} & \Delta f > f_{max} \\ x_k^{init} + \left(x_k^{min} - x_k^{init}\right)\frac{\Delta f - f_d^+}{f_{max} - f_d^+} & f_d^+ < \Delta f \le f_{max} \\ x_k^{init} & f_d^- \le \Delta f \le f_d^+ \quad x_k \in \chi_{dec}. \\ x_k^{init} - \left(x_k^{init} - x_k^{max}\right)\frac{\Delta f - f_d^-}{f_{min} - f_d^-} & f_{min} \le \Delta f < \Delta f_d^- \\ x_k^{max} & \Delta f < f_{min} \end{cases} \quad (17)$$

As indicated in (13) and (15), the x_k^{max} and x_k^{min} in Fig. 4 can be determined analytically with local information. The initial operating point of the ES is set to half of the maximum power in order to provide equal up and down regulation ability for maximizing the utility of the ES under the frequency support mode. Consequently, x_k^{init} can be solved as follows,

$$x_k^{init} = \frac{\tan\varphi_{NCL} \pm 1}{\sqrt{2}}. \quad (18)$$

The sign in (18) is positive for $\varphi_k^{NCL} \in \left[-\frac{\pi}{2}, 0\right)$ and it is negative for $\varphi_k^{NCL} \in \left(0, \frac{\pi}{2}\right]$. Further, $x_k^{init} = \pm\frac{1}{\sqrt{2}}$ for $\varphi_k^{NCL} = 0$. A controller is proposed to control x_k in order to facilitate the frequency control of the microgrid as shown in Fig. 5.

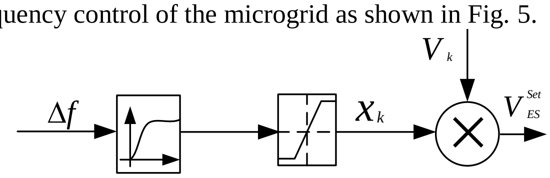

Fig. 5. Proposed control strategy of the ES under frequency support mode.

As shown in Fig. 5, Δf can be measured locally and x_k can be obtained by (16) and (17). The operation limits can be calculated by (13), (15), and (18) with the local information.

C. ES with a Weak Bus and Operated Locally

If the CL installed with the ES is located far away from the controllable generators or the voltage compensation devices, the bus voltage on the CL may greatly vary with the operation of the ES. The bus voltage in (10) may not be considered as a constant anymore and the communication system may not be available after an extreme natural event. In this case, the ES should regulate the system frequency by guaranteeing the voltage on the CL within the specified region with the local information.

Referring to Fig. 3, the lower arc of the ES P-V curve is used in order to maximize the utility of frequency regulation when the ES is connected with a strong bus. The upper arc in Fig. 3 is selected to increase the voltage level when the bus voltage is lower than the nominal value for most resistive and inductive loads without an ES. Otherwise, the lower arc of the ES is selected.

When the upper arc is selected, the calculation of x_k^{min} and x_k^{max} gives the same results as in (13) and (15) for the resistive NCLs. However, x_k^{init} is equal to $-\frac{1}{\sqrt{2}}$. For the inductive and capacitive NCLs, the calculation of x_k^{max} yields the same result as in (13), while x_k^{min} and x_k^{init} are different due to the γ_k can not be reduced to zero. They are represented as follows and the details of derivations are stated in the Appendix.

$$x_k^{min} = \mp\frac{1}{\cos\varphi_k^{NCL}} \quad (19)$$

$$x_k^{init} = \frac{\tan\varphi_{NCL}\sqrt{1+\sin^2\varphi_k^{NCL}} \mp \cos\varphi_k^{NCL}}{\sqrt{2}}. \quad (20)$$

where, the sign in (19) and (20) is negative for $\varphi_k^{NCL} \in \left[-\frac{\pi}{2}, 0\right)$ and it is positive for $\varphi_k^{NCL} \in \left(0, \frac{\pi}{2}\right]$.

In order to consider the voltage constraints on CLs locally, the local controller sets operation limits on x_k as the value of the last control interval when the bus voltage V_k reaches the operation limits.

Considering the effects of ES operation on the bus voltage, the maximum power consumed by the bus with an ES may be different from (14). Thus, the operating limit of x_k may also be different from (13). Consequently, a detector unit is added in the local controller to monitor the sign of $d(P_k^{CL} + P_k^{NCL})/dx_k$. When it equals zero, the operating limits of x_k are replaced by the current value of x_k in order to avoid x_k exceeding the monotone interval.

IV. Operation of the ES with a Communication System

When the communication system of an ES is available after extreme natural events, the interactions of the ES with other elements in the microgrid can be considered by calculating the AC power flows. The bus voltage and the active power consumed by the buses with ESs can be calculated accurately. An optimization model is proposed as the controller of the microgrid to determine the operation limits and the initial operating set points for the ESs in order to maximize the utility to regulate the system frequency for the microgrid by considering the voltage constraints on the CLs.

A. Constraints

The AC power flows that are considered in the proposed model and the buses without installing an ES can be expressed as follows,

$$P_i^G - P_i^D = V_i \sum_{j=1}^{NB} V_j\left(G_{ij}\cos\delta_{ij} + B_{ij}\sin\delta_{ij}\right) \quad (21)$$

$$Q_i^G - Q_i^D = V_i \sum_{j=1}^{NB} V_j\left(-B_{ij}\cos\delta_{ij} + G_{ij}\sin\delta_{ij}\right), \quad (22)$$

In this paper, the generation resources and the ES are assumed as not being installed on the same bus, which is represented by the subscript *k*. It means that $P_k^G = 0$. The power flow equations on the bus installed with an ES can be expressed as follows,

$$\frac{{V_k^{NCL}}^2 R_k^{NCL}}{{Z_k^{NCL}}^2} + \frac{{V_k}^2 R_k^{CL}}{{Z_k^{CL}}^2} = -V_k \sum_{j=1}^{NB} V_j\left(G_{kj}\cos\delta_{kj} + B_{kj}\sin\delta_{kj}\right) \quad (23)$$

$$\frac{V_k^{NCL}}{Z_k^{NCL}} V_k^{ES} + \frac{{V_k^{NCL}}^2 X_k^{NCL}}{{Z_k^{NCL}}^2} + \frac{{V_k}^2 X_k^{CL}}{{Z_k^{CL}}^2} = -V_k \sum_{j=1}^{NB} V_j \times \left(-B_{kj}\cos\delta_{kj} + G_{kj}\sin\delta_{kj}\right). \quad (24)$$

Equations (23) and (24) can be modified as follows,

$$\frac{V_k\left(\sin\varphi_k^{NCL} x_k + \sqrt{1-\cos^2\varphi_k^{NCL} {x_k}^2}\right)^2 R_k^{NCL}}{{Z_k^{NCL}}^2} + \frac{V_k R_k^{CL}}{{Z_k^{CL}}^2} = -\sum_{j=1}^{NB} V_j\left(G_{kj}\cos\delta_{kj} + B_{kj}\sin\delta_{kj}\right) \quad (25)$$

This article has been accepted for publication in a future issue of this journal, but has not been fully edited. Content may change prior to final publication. Citation information: DOI 10.1109/TSG.2016.2609603, IEEE Transactions on Smart Grid

$$\frac{V_k\left(\sin\varphi_k^{NCL}x_k+\sqrt{1-\cos^2\varphi_k^{NCL}x_k{}^2}\right)}{Z_k^{NCL}}x_k+\frac{V_k\left(\sin\varphi_k^{NCL}x_k+\sqrt{1-\cos^2\varphi_k^{NCL}x_k{}^2}\right)^2 X_k^{NCL}}{Z_k^{NCL^2}} + \frac{V_k X_k^{CL}}{Z_k^{CL^2}} = -\sum_{j=1}^{NB} V_j\left(-B_{kj}\cos\delta_{kj}+G_{kj}\sin\delta_{kj}\right). \quad (26)$$

Comparing with (23) and (24), the order of V_k in (25) and (26) is reduced. The voltages on the CLs are constrained as follows,

$$V_k^{min} \le V_k \le V_k^{max}. \quad (27)$$

The operating region of x_k can be constrained as follows,

$$x_k^{lo} \le x_k \le x_k^{up}. \quad (28)$$

B. Objective Function

The four vertices of the curves in Fig. 3 are essential to determine the operating limits of the ES. The locations of these vertices can be calculated by the proposed models with the following objective functions.

$$C_1 = maxP_k^D\ , \quad (29)$$

$$C_2 = minP_k^D\ , \quad (30)$$

$$C_3 = maxV_k, \quad (31)$$

and

$$C_4 = minV_k. \quad (32)$$

The consumed active powers under the maximum and minimum consumed active power calculated by (29) and (30) are represented by $P_k^{D,max}$ and $P_k^{D,min}$, respectively.

C. Solution Method

Based on the different relationships between the voltage vertices of the ES and the voltage constraints on the CL, the calculation of the operation limits of an ES can be classified into four groups as shown in Fig. 6.

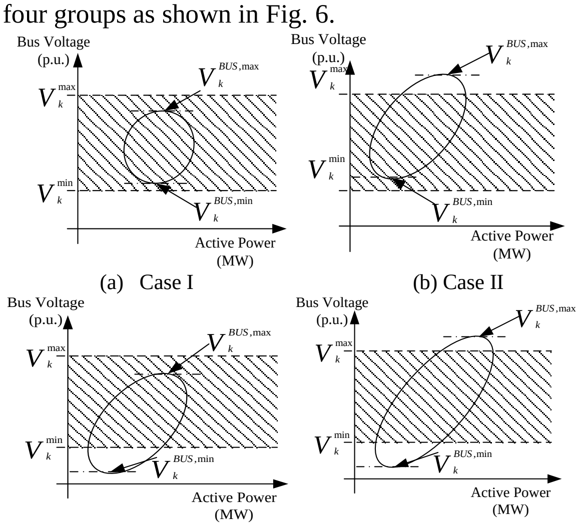

(a) Case I (b) Case II (c) Case III (d) Case IV

Fig. 6. Different operation limits of the ES considering voltage constraints.

As shown in Fig. 6(a), the acceptable voltage region is represented by a shadow area between the upper and lower boundaries indicated by V_k^{max} and V_k^{min}. When both the $V_k^{BUS,min}$ and $V_k^{BUS,max}$ are located within the acceptable voltage region, the x_k^{max} and x_k^{min} solved by $P_k^{BUS,min}$ and $P_k^{BUS,max}$ without considering the voltage constraints can be used as the operation limits of the ES. The operating curves of an ES with resistive and inductive NCLs are continuous arcs at the lower part so that the unclosed parts always exist at the upper part of the curves. As shown in Fig. 6(b), when $V_k^{BUS,max}$ is located outside the acceptable voltage region, the feasible region of x_k is a connected set and x_k^{max} and x_k^{min} are required to be solved with the secured voltage constraints. As shown in Figs. 6(c) and 6(d), when the $V_k^{BUS,min}$ or both the $V_k^{BUS,min}$ and $V_k^{BUS,max}$ are located outside the secured voltage region, the feasible regions of x_k are not connected sets and they are divided into two parts as two connected sets in the shadow area. The two arcs are divided by x_k^{up} and x_k^{lo}, which are obtained by solving the two vertices, $V_k^{BUS,min}$ and $V_k^{BUS,max}$. As a result, an additional constraint of x_k^{up} and x_k^{lo} is added to solve $P_k^{BUS,min}$ and $P_k^{BUS,max}$ in each connected set of x_k. Further, the arc with a higher value of $P_k^{BUS,max} - P_k^{BUS,min}$ is selected as the operating region of the ES because of its greater regulation ability. The solving method can be described by the pseudo-code as follows.

TABLE II
PSEUDO-CODE FOR CALCULATING X_K AND X_{INIT}

(1)	Solving the $V_k^{BUS,min}$, $V_k^{BUS,max}$, $P_k^{BUS,min}$, $P_k^{BUS,max}$ without constraints on voltage and x_k with (21)-(22), (25), (26) and (29)-(32)
(2)	If both $V_k^{BUS,min}$ and $V_k^{BUS,max}$ are within 1 ± 0.1p.u. then
(3)	Solving the operation limits on x_k and x_{init} with $P_k^{BUS,min}$ and $P_k^{BUS,max}$.
(4)	Else
(5)	If both $V_k^{BUS,min}$ and $V_k^{BUS,max}$ are exceed 0.1p.u. then
(6)	Solving the $P_k^{D,min}$ and $P_k^{D,max}$ with constraints on voltage and x_k using (21),(22), (25)-(28), and (31)-(32) for both arcs.
(7)	Solving the operation limits on x_k and x_{init} with $P_k^{D,min}$ and $P_k^{D,max}$ on the arc with larger $P_k^{D,min} - P_k^{D,max}$.
(8)	Else
(9)	If the $\varphi_k^{NCL} = 0$ or $V_k^{BUS,min}$ >-0.1 p.u. then
(10)	Solving the $P_k^{D,min}$ and $P_k^{D,max}$ with constraints on voltage and x_k using (21),(22), (25)-(27), and (31)-(32) for both arcs.
(11)	Solving the operation limits on x_k and x_{init} with $P_k^{D,min}$ and $P_k^{D,max}$ with larger $P_k^{D,min} - P_k^{D,max}$.
(12)	Else
(13)	Solving the $P_k^{D,min}$ and $P_k^{D,max}$ with constraints on voltage and x_k using (21),(22), (25)-(28), and (31)-(32) for both arcs
(14)	Solving the operation limits on x_k and x_{init} with $P_k^{D,min}$ and $P_k^{D,max}$ with larger $P_k^{D,min} - P_k^{D,max}$.
(15)	End
(16)	End
(17)	End

Finally, the initial operating set point of ES can be calculated by solving (21), (22), (25), and (26) with $P_k^{D,max}$, $P_k^{D,min}$, and $P_k^{init} = \frac{\left(P_k^{D,max}+P_k^{D,min}\right)}{2}$.

V. CASE STUDY

In the case studies, the effectiveness of an ES with the proposed operating strategy is verified in different situations. In the first case, in order to study the maximal utility of ESs for regulating system frequency, the voltage constraints on the CLs are not considered. In this way, both of the CLs and NCLs are involved to regulate system frequency. In the second case, the voltage constraints on the CLs are considered to make sure the CLs can be reliably supplied. For both cases, the results of the ES with and without communication systems are carried out. In the third case, it is assumed a CL can not be supplied by its original microgrid after extreme natural events. The CL is

This article has been accepted for publication in a future issue of this journal, but has not been fully edited. Content may change prior to final publication. Citation information: DOI 10.1109/TSG.2016.2609603, IEEE Transactions on Smart Grid

supplied by another microgrid through the available distribution network. The voltage on the CL is regulated within the acceptable region by the ES under voltage support mode. The utility of voltage support of the ES is discussed under different configuration of CL and NCL. A 13-bus microgrid is employed as shown in Fig. 7. The line parameters and rated voltage of the microgrid can be found in [19]. The base value of apparent power is 10 MVA. The diesel generator controls the voltage of bus #1 to the nominal value of 1 p.u. during the simulation. A PV station is located at bus #2. A 1000 second historical PV output profile from the EPRI website [20] as in Fig. 8 is studied in the case studies. A classical automatic generation control (AGC) scheme with load characteristics described by parameters, *D* and *M*, as in [21] is applied for the diesel generator to regulate the frequency. The loads, line parameters, and the simulation parameters are described in the Appendix. In order to demonstrate the utility of the ES under the proposed strategy more clearly, the voltage deviations for the bus #13 without an ES are designed to large values in the case studies.

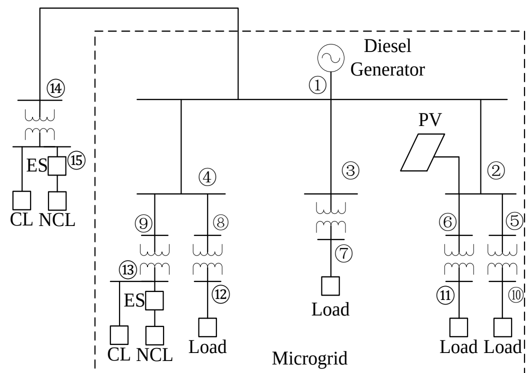

Fig. 7. System topology of a 13-bus microgrid and a CL.

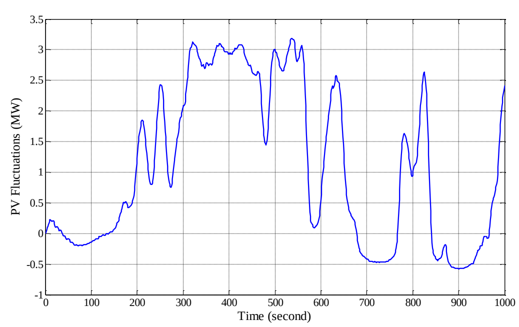

Fig. 8. Historical PV scenario.

A. Operating Traces of an ES at Bus #13 with NCLs of Different Power Factors

For the case studies, the operating traces of an ES located at bus #13 with NCLs of two power angles, $\varphi_k^{NCL} = 0$ and $\varphi_k^{NCL} = -\pi/6$, are shown in Fig. 9 and Fig. 10 respectively.

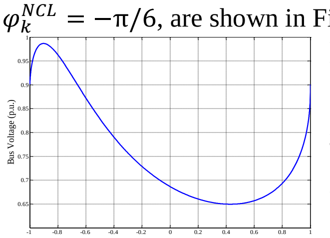
(a) The curve between V_{13} and x_{13}

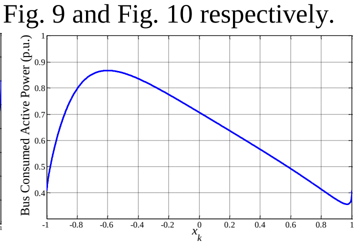
(b) The curve between P_{13}^D and x_{13}

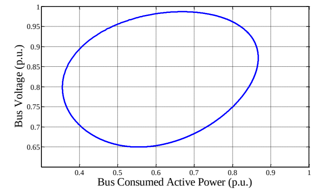
(c) The power-voltage curve of bus #13

Fig. 9 The curves of bus #13 with a NCL of $\varphi_k^{NCL} = 0$

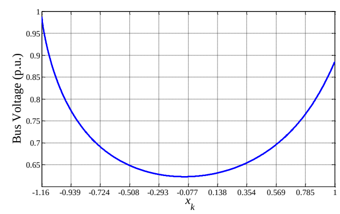
(a) The curve between V_{13} and x_{13}

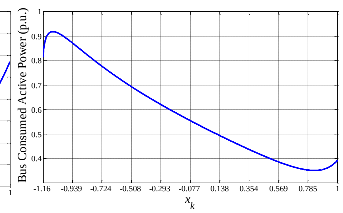
(b) The curve between P_{13}^D and x_{13}

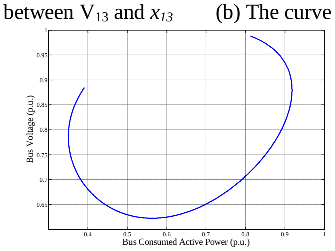
(c) The power-voltage curve of bus #13

Fig. 10 The curves of bus #13 with a NCL of $\varphi_k^{NCL} = -\pi/6$

As shown in Fig. 9(c), the operating trace of an ES with a resistive NCL is a closed curve. While as shown in Fig. 10(c), the operating trace of an ES with an inductive NCL with a power angle of $\varphi_k^{NCL} = -\pi/6$ is not a closed curve due to the different feasible operating regions of x_k with NCLs of different power angles. An inductive NCL causes a lower minimum bus voltage than a resistive NCL as shown in Fig. 9(a) and Fig. 10(a). By considering voltage constraints on CLs at bus #13, the utility of an ES for frequency regulation is lower with an inductive NCL than a resistive NCL as shown in Fig. 9(c) and Fig. 10(c).

B. Case #1, ES under Frequency Support Mode for CLs without Voltage Constraints

In the first case, the voltage constraints on the CLs are not considered. It means that both the NCL and the CL can be used as operating resources to regulate the system frequency. The mean absolute frequency deviations (MAFD), the maximum positive frequency deviations (MPFD), and the minimum negative frequency deviations (MNFD) are calculated and shown in Table III. Most frequency indices can be reduced more than 40% by installing an ES.

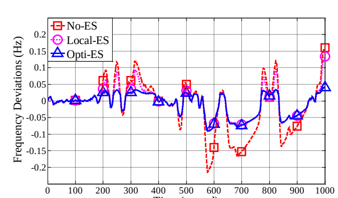

(a) $\varphi_k^{NCL} = 0$

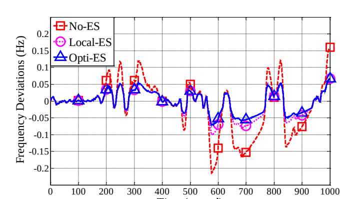

(b) $\varphi_k^{NCL} = -\pi/6$

Fig. 11. Frequency deviations with different φ_k^{NCL}.

This article has been accepted for publication in a future issue of this journal, but has not been fully edited. Content may change prior to final publication. Citation information: DOI 10.1109/TSG.2016.2609603, IEEE Transactions on Smart Grid

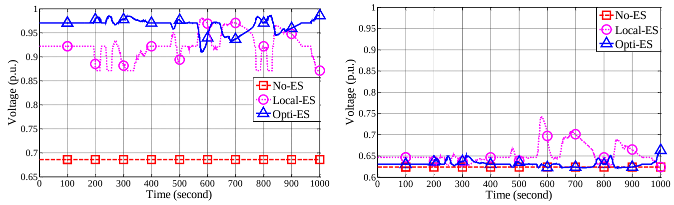

(a) $\varphi_k^{NCL} = 0$ (b) $\varphi_k^{NCL} = -\pi/6$

Fig. 12. Voltage deviations with different φ_k^{NCL}.

TABLE III
RESULTS OF FREQUENCY DEVIATIONS

φ_k^{NCL}		MAFD (Hz)	%[a]	MPFD (Hz)	%[a]	MNFD(Hz)	%[a]
0	No-ES	0.0530	100	0.1600	100	-0.2140	100
	Local-ES	0.0319	60.2	0.1336	83.5	-0.0855	40.0
	Opti-ES	0.0268	50.6	0.0407	25.4	-0.0911	42.6
$-\pi/6$	No-ES	0.0530	100	0.1600	100	-0.2140	100
	Local-ES	0.0292	55.1	0.0667	41.7	-0.0995	46.5
	Opti-ES	0.0256	48.3	0.0666	41.6	-0.0702	32.8

Note. [a]The value of No-ES is regarded as 100%

As shown in Figs. 11 and 12, the solid line with triangle marks, the dot line with circle marks, and the dash line with square marks represent the frequency deviations and voltage deviations on bus #13 with the operation limits obtained by the proposed optimization model, the local controller, and with no ES, respectively. The frequency and the voltage deviations indicate that the ES with a communication system can determine the initial operating points with equivalent up and down regulation capability and further, achieve the best performance. The operation limits obtained from the local controller are not accurate owing to the variation of the bus voltage, while it can reduce the frequency deviations in comparison to the results without installing an ES. As shown in Fig. 12, the ES can also improve the voltage quality on the CL both under the local controller and the optimization model for the resistive NCLs by selecting the upper operating arc as indicated in Figs. 3 and Figs. 6. While for the inductive NCLs, the ES could not improve the voltage quality on the CL owing to maximize the utility for frequency regulation by selecting the lower arc as indicated in Figs. 3 and Figs. 6.

C. Case #2, ES under Frequency Support Mode for CLs with Voltage Constraints

In the second case, the acceptable voltage deviations on the CL are set to ± 0.1 p.u. When the voltage on the CL exceeds this region, the local controller will set the current x_k as the operating limit and the following x_k can only be varied in another direction in order to make the voltage on the CL remain within the acceptable region. The same PV scenario as shown in Fig. 8 is applied in this case. Although the utility of ES for frequency regulation is reduced by considering voltage constraints, the most frequency indices can be reduced more than 10% by installing ES, especially for the ES with communication system.

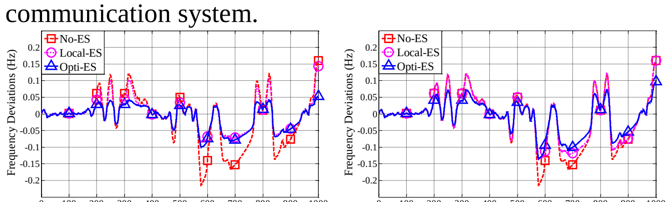

(a) $\varphi_k^{NCL} = 0$ (b) $\varphi_k^{NCL} = -\pi/6$

Fig. 13. Frequency deviations with different φ_k^{NCL}.

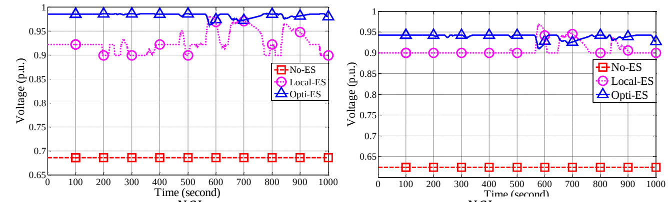

(a) $\varphi_k^{NCL} = 0$ (b) $\varphi_k^{NCL} = -\pi/6$

Fig. 14. Voltage deviations with different φ_k^{NCL}.

TABLE IV
RESULTS OF FREQUENCY DEVIATIONS

φ_k^{NCL}		MAFD (Hz)	%[a]	MPFD (Hz)	%[a]	MNFD(Hz)	%[a]
0	No-ES	0.0530	100	0.1600	100	-0.2140	100
	Local-ES	0.0334	63.0	0.1436	89.8	-0.0855	40.0
	Opti-ES	0.0287	54.2	0.0527	32.9	-0.1001	46.8
$-\pi/6$	No-ES	0.0530	100	0.1600	100	-0.2140	100
	Local-ES	0.0477	90.0	0.1600	100	-0.1370	64.0
	Opti-ES	0.0368	69.4	0.0968	60.5	-0.1352	63.2

Note. [a]The value of No-ES is regarded as 100%

As shown in Fig. 13, Fig. 14, and the calculation results in Table IV, the frequency deviations and the voltage deviations can be reduced with the ES. The local controller and the controller with the optimization model can regulate the system frequency by controlling the voltage deviations on the CLs within $\pm$ 0.1 p.u. The proposed optimization model can determine the operating limits effectively for both the resistive and the inductive NCLs by considering voltage constraints on the CLs and further, achieve the best performance as shown in Figs. 13 and 14. Comparing with the resistive NCLs, the inductive NCLs makes the bus voltage lower than the resistive NCLs and reduce the feasible operating region of the ES; thus, the utility of the ES for frequency regulation is reduced, especially for the inductive NCLs with the bus voltage lower than the nominal value.

D. Case #3, ES under Voltage Support Mode for CLs with Weak Connection

In the third case, it is assumed that an ES is installed on the bus #15 with a CL outside the microgrid. The CL is proposed to be supplied by the available microgrid as in Fig. 7 after an extreme natural event. The connection between the CL and the available microgrid is so weak that the voltage deviations on the bus #15 are larger than $\pm$0.1 p.u. Hence, the ES installed on bus #15 is operated under the voltage support mode in order to regulate the bus voltage on the CL. The summation of the NCL and the CL equals 2 MW. The effects of the ratio of the NCL to the total bus load on the bus voltage level is studied in this case and the results are shown in Fig. 15.

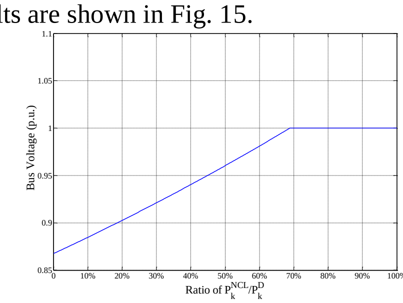

Fig. 15. Voltage control results of bus #15 with an ES.

As shown in Fig. 15, with the facilitation of the ES, the voltage on bus #15 can be improved. With an increase in the ratio of the NCL to the total load, the voltage deviations can be

This article has been accepted for publication in a future issue of this journal, but has not been fully edited. Content may change prior to final publication. Citation information: DOI 10.1109/TSG.2016.2609603, IEEE Transactions on Smart Grid

reduced accordingly. In this case, when the ratio is about 20%, the bus voltage can be regulated within ± 0.1 p.u. and when the ratio is larger than 70%, the bus voltage can be regulated to the nominal value.

E. Discussions

The ES can regulate the system frequency and the bus voltage on the CL effectively, especially with the existence of a communication system. Comparing with the voltage support mode of the ES, the proposed frequency support mode can regulate the system frequency by releasing the voltage on the CL from a constant value to an acceptable region. When the bus voltage is lower than the nominal value, the ES can be operated more effectively with the resistive NCLs than the inductive NCLs in order to regulate the system frequency. The ES under voltage support mode can supply the CLs with other microgrids through weak connections.

VI. Conclusions

In this paper, a control strategy has been developed for ES to enhance the resilience of microgrids by coordinating voltage and frequency control. Several essential conclusions are obtained as follows,

(1) The NCLs connected with ES can be controlled by the ESs and enhance the resilience of microgrid. The feasible operating region of the ES output voltage is derived as a closed form of the power factor of the NCL connected with the ES. When the NCL is a resistive load, the feasible operating region of the ES is symmetrical and the *P-V* curve of the bus connected with the ES is similar to a closed ellipse. When the NCL is an inductive or a capacitive load, the feasible operating region of the ES is asymmetrical and the *P-V* curve of the bus connected with the ES is an unclosed arc.

(2) When the bus connected with the ES is strong and the bus voltage can be considered as a constant during the operating of the ES, the operating limits and the initial operating set points of the ES for the proposed control strategy can be represented analytically. Consequently, the ES can be operated with the local information under the proposed frequency support mode.

(3) When the bus connected with the ES is weak and the bus voltage is highly variable with the operation of the ES, the operating limits, and the initial set points for the proposed control strategy cannot be accurately obtained with local information. The existence of a communication system can improve the operating performance of the ES by providing the global operating information of the microgrid to calculate the operating limits and the initial set points for the ES by the proposed optimization model.

(4) The ES can improve the voltage quality on the CL under the voltage support mode. With an increasing ratio of the NCL to the total bus load, the operating performance of the ES can be improved.

(5) The frequency deviations and the voltage deviations on the CLs caused by the fluctuating renewable energy after extreme natural events can be reduced by installing ESs in the microgrids and further, the CL can be reliably supplied within the microgrid under islanded mode so that the system resilience can be enhanced.

Based on the above conclusions, it is shown that the frequency support mode and the voltage support modes of the ES can assure reliable supply of CLs after extreme natural events and can improve the resilience of a microgrid.

References

[1] NERC, "Severe Impact Resilience: Considerations and Recommendations," USA, Tech Rep, May. 2012. [Online]. Available: http://www.nerc.com/docs/oc/sirtf/SIRTF_Final_May_9_2012-Board_Accepted.pdf

[2] Office of the Press Secretary, "Presidential Policy Directive 21 - Critical Infrastructure Security and Resilience," The Whit House, DC, USA, Feb. 2013. [Online]. Available: https://www.whitehouse.gov/the-press-office-/2013/02/12/presidential-policy-directive-critical-infrastructuresecurity-and-resil

[3] S. D. Manshadi and M. E. Khodayar, "Resilient Operation of Multiple Energy Carrier Microgrids," *IEEE Trans. Smart Grid*, vol. 6, no. 5, pp. 2283-2292, Sep. 2015.

[4] M. Simonov, "Dynamic Partitioning of DC Microgrid in Resilient Clusters Using Event-Driven Approach," *IEEE Trans. Smart Grid*, vol. 5, no.5, pp. 2618-2625, Sep. 2014.

[5] L. Che and M. Shahidehpour, "DC Microgrids: Economic Operation and Enhancement of Resilience by Hierarchical Control," *IEEE Trans. Smart Grid*, vol. 5, no. 5, pp. 2517-2526, Sep. 2014.

[6] J. Morren, S. W. H. de Haan, W. L. Kling, and J. A. Ferreira, "Wind turbines emulating inertia and supporting primary frequency control," *IEEE Trans. Power Syst*., vol. 21,no. 1, pp. 433-434, Feb. 2006.

[7] M. J. Hossain, H. R. Pota, M. A. Mahmud, and M. Aldeen, "Robust Control for Power Sharing in Microgrids With Low-Inertia Wind and PV Generators," *IEEE Trans. Sustain. Energy*, vol. 6, no. 3, pp. 1067-1077, Jul. 2015.

[8] I. Serban and C. Marinescu, "Control Strategy of Three-Phase Battery Energy Storage Systems for Frequency Support in Microgrids and with Uninterrupted Supply of Local Loads," *IEEE Trans. Power Electron.*, vol. 29, no. 9, pp. 5010-5020, Sep. 2014.

[9] E. Planas, A. Gil-de-Muro, J. Andreu, I. Kortabarria, Marti, x, et al., "Design and implementation of a droop control in d-q frame for islanded microgrids," *IET Renew Power Gen.*, vol. 7, no. 5, pp. 458-474, Feb. 2013.

[10] F. F. Wu, P. P. Varaiya, and R. S. Y. Hui, "Smart Grids with Intelligent Periphery: An Architecture for the Energy Internet," *Engineering*, vol. 1, no. 4, pp. 436-446, Dec. 2015.

[11] M. Aunedi, P. A. Kountouriotis, J. E. O. Calderon, D. Angeli, and G. Strbac, "Economic and Environmental Benefits of Dynamic Demand in Providing Frequency Regulation," *IEEE Trans. Smart Grid*, vol. 4, no. 4, pp. 2036-2048, Dec. 2013.

[12] S. Y. Hui, C. K. Lee, and F. F. Wu, "Electric Springs-A New Smart Grid Technology," *IEEE Trans. Smart Grid*, vol. 3, no. 3, pp. 1552-1561, Sep. 2012.

[13] S. C. Tan, C. K. Lee, and S. Y. Hui, "General Steady-State Analysis and Control Principle of Electric Springs With Active and Reactive Power Compensations," *IEEE Trans. Power Electron.*, vol. 28, no. 8, pp. 3958-3969, Aug. 2013.

[14] X. Chen, Y. Hou, S. C. Tan, C. K. Lee, and S. Y. R. Hui, "Mitigating Voltage and Frequency Fluctuation in Microgrids Using Electric Springs," *IEEE Trans. Smart Grid*, vol. 6, no. 2, pp. 508-515, Mar. 2015.

[15] X. Luo, Z. Akhtar, C. K. Lee, B. Chaudhuri, S. C. Tan, and S. Y. R. Hui, "Distributed Voltage Control with Electric Springs: Comparison with STATCOM," *IEEE Trans. Smart Grid*, vol. 6, no. 1, pp. 209-219, 2015.

[16] Z. Akhtar, B. Chaudhuri, and S. Y. Hui, "Primary Frequency Control Contribution From Smart Loads Using Reactive Compensation," *IEEE Trans. Smart Grid*, vol. 6, no. 5, pp. 2356-2365, Sep. 2015.

[17] C. K. Lee and Y. S, "Reduction of Energy Storage Requirements in Future Smart Grid Using Electric Springs," *IEEE Trans. Smart Grid*, vol. 4, no. 3, pp. 1282-1288, 2013.

[18] P. Karlsson and J. Svensson, "DC bus voltage control for a distributed power system," *IEEE Trans. Power Electron*, vol. 18, no. 6, pp. 1405-1412, 2003.

[19] F. Katiraei, M. R. Iravani, and P. W. Lehn, "Micro-grid autonomous operation during and subsequent to islanding process," *IEEE Trans. Power Del.*, vol. 20, no. 1, pp. 248-257, Jan. 2005.

[20] PV operating data. [Online]. Available: http://dpv.epri.com/measurement-_data.html

[21] P. Kundur, N. J. Balu, and M. G. Lauby, "Power system stability and control," vol. 7, New York:McGraw-Hill, 1994.

This article has been accepted for publication in a future issue of this journal, but has not been fully edited. Content may change prior to final publication. Citation information: DOI 10.1109/TSG.2016.2609603, IEEE Transactions on Smart Grid

APPENDIX

TABLE V
PARAMETERS OF THE MICROGRID

Line	1	2
Start Bus	1	14
End Bus	14	15
R (p.u.)	0.6	0.0329
L (p.u.)	1.2	0.0203

TABLE VI
BUS LOAD OF THE MICROGRID

Bus No.	7	10	11	12	13	15
Load (MW, MVar)	2+0.3j	3+0.3j	2+0.4j	3+0.5	0.2+0.1j	2

TABLE VII
SIMULATION PARAMETERS

M	D	f_d^+, f_d^-	f_{up}, f_{lo}	S_{Diesel}	Z_{NCL}	R_{CL}
6.5	10	±0.02Hz	±0.15Hz	30MWA	1	2

A. Derivation of Solutions Selection

The V_k^{NCL} and γ_k shown in (7) and (8) may have two possible solutions. For a resistive NCL with $\sin\varphi_k^{NCL} = 0$, it is obvious that only the positive value can be selected as the solution for V_k^{NCL} and γ_k. However, for an inductive or a capacitive NCL, all solutions of (7) and (8) can be positive. In this way, it is not obviously to choose the reasonable solution from the two solutions. The derivations of selecting the reasonable solution are represented with an inductive NCL under capacitive mode. The solutions for an inductive NCL under inductive mode and a capacitive NCL under both modes can be obtained with the same derivations.

For an ES with an inductive NCL under capacitive mode, both possible solutions for V_k^{NCL} are shown in Fig. A1 and marked as V_k^{NCL} and V'^{NCL}_k respectively. When an ES is deactive, the output of an ES, V_k^{ES}, is set to zero. With the increasing of the V_k^{ES}, the V_k^{NCL} should be achieved earlier than V'^{NCL}_k and the upper limit of V_k^{ES}/V_k, in this case it equals to 1, will be reached earlier than achieving V'^{NCL}_k. Consequently, V'^{NCL}_k is not a possible solution and V_k^{NCL} should be selected as the only solution for (7) and (8).

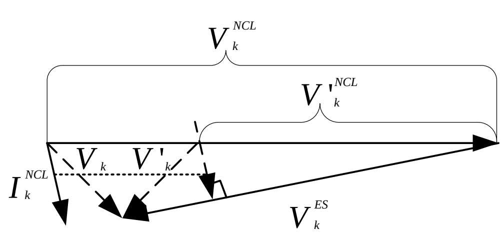

Fig. A1. Vector diagram of possible solutions

B. Derivation of the Characteristic of Power-Voltage Curve

Considering a two bus system, where the bus #1 is an infinite bus and its voltage equals 1 p.u. An ES is connected to bus #2 with a NCL. A CL is connected with bus #2 directly. According to (21) and (22), the power flow equations are listed as follows,

$$-P_2^D = V_2 \sum_{j=1}^{NB} V_j\left(G_{2j}\cos\delta_{2j} + B_{2j}\sin\delta_{2j}\right) \quad \text{(A1)}$$

$$-Q_2^D = V_2 \sum_{j=1}^{NB} V_j\left(-B_{2j}\cos\delta_{2j} + G_{2j}\sin\delta_{2j}\right), \quad \text{(A2)}$$

where, $P_2^D = P_2^{NCL} + P_2^{CL}$, $Q_2^D = Q_2^{NCL} + Q_2^{ES} + Q_2^{CL}$, and $V_1 = 1$. Considering a resistive NCL, (25) and (26) can be represented as follows,

$$\frac{V_2(1-x_2^2)}{R_2^{NCL}} + \frac{V_2 R_2^{CL}}{Z_2^{CL^2}} = -(G_{21}\cos\delta_{21} + B_{21}\sin\delta_{21}) - V_2 G_{22} \quad \text{(A3)}$$

$$\frac{V_2\sqrt{(1-x_2^2)}x_2}{R_2^{NCL}} + \frac{V_2 X_2^{CL}}{Z_2^{CL^2}} = -(-B_{21}\cos\delta_{21} + G_{21}\sin\delta_{21}) + V_2 B_{22}, \quad \text{(A4)}$$

where $x_2 \in [-1,1]$, G_{22} is positive while B_{22} is negative. Let $\mathrm{CP}_1 = 1 + \frac{R_2^{NCL}R_2^{CL}}{Z_2^{CL^2}} + R_2^{NCL}G_{22}$ and $\mathrm{CP}_2 = \frac{R_2^{NCL}X_2^{CL}}{Z_2^{CL^2}} - R_2^{NCL}B_{22}$, (A5) can be obtained as the summation of the squares of (A3) and (A4) as follows,

$$\frac{V_2^2(\mathrm{CP}_1 - x_2^2)^2}{R_2^{NCL^2}} + \frac{V_2^2(\mathrm{CP}_2 + \sqrt{(1-x_2^2)}x_2)^2}{R_2^{NCL^2}} = G_{21}^2 + B_{21}^2. \quad \text{(A5)}$$

Let $z = V_2^2$, (A5) can be reformed as follows,

$$\frac{z(\mathrm{CP}_1 - x_2^2)^2 + z(\mathrm{CP}_2 + \sqrt{(1-x_2^2)}x_2)^2}{R_2^{NCL^2}(G_{21}^2 + B_{21}^2)} = 1. \quad \text{(A6)}$$

Let $c = R_2^{NCL^2}(G_{21}^2 + B_{21}^2)$, (A7) can be obtained as follows,

$$z = \frac{c}{(\mathrm{CP}_1 - x_2^2)^2 + (\mathrm{CP}_2 + \sqrt{(1-x_2^2)}x_2)^2}. \quad \text{(A7)}$$

Let $y = (\mathrm{CP}_1 - x_2^2)^2 + (\mathrm{CP}_2 + \sqrt{(1-x_2^2)}x_2)^2$, the first and third derivatives of $y(x_2)$ are represented as follows,

$$\frac{dy}{dx_2} = 2x_2 - 4\mathrm{CP}_1 x_2 + 2\mathrm{CP}_2\sqrt{(1-x_2^2)} - \frac{2\mathrm{CP}_2 x_2^2}{\sqrt{(1-x_2^2)}} \quad \text{(A8)}$$

$$\frac{d^3y}{dx_2^3} = \frac{-6\mathrm{CP}_2}{\sqrt{(1-x_2^2)^5}} < 0 \quad (x_2 \in [-1,1]). \quad \text{(A9)}$$

Owing to the third derivative of $y(x_2)$ is negative for $x_2 \in [-1,1]$, the first derivative of $y(x_2)$ is concave. Furthermore, considering $\left.\frac{dy}{dx_2}\right|_{x_2=\pm1} = -\infty$ and $\left.\frac{dy}{dx_2}\right|_{x_2=0} = 2\mathrm{CP}_2 > 0$, the first derivate should equal to zero for two times. As a consequence, the y should achieve its minimal and maximal value for $x_2 \in [-1,1]$ only one time respectively. The maximal and minimal value of y are the maximum and minimum value respectively. Furthermore, z and V_2 should achieve its minimal and maximal value for $x_2 \in [-1,1]$ only one time respectively. The shape of the graph between V_2 and x_2 is similar to Fig. 9(a).

Consider $\frac{V_2^2(1-x_2^2)}{R_2^{NCL}} + \frac{V_2^2 R_2^{CL}}{Z_2^{CL^2}} = P_2^D$ and let $\mathrm{CP}_3 = \left(\frac{1}{R_2^{NCL}} + \frac{R_2^{CL}}{Z_2^{CL^2}}\right)$, equation (A10) can be obtained as follows,

$$P_2^D = \frac{\frac{c}{R_2^{NCL}}\left(R_2^{NCL}\mathrm{CP}_3 - x_2^2\right)}{(\mathrm{CP}_1 - x_2^2)^2 + (\mathrm{CP}_2 + \sqrt{(1-x_2^2)}x_2)^2}. \quad \text{(A10)}$$

Consider $R_2^{NCL}\mathrm{CP}_3 = 1 + \frac{R_2^{NCL}R_2^{CL}}{Z_2^{CL^2}} > 1$ and $x_2 \in [-1,1]$,

$$0 < \left(R_2^{NCL}\mathrm{CP}_3 - x_2^2\right) \leq 1 + \frac{R_2^{NCL}R_2^{CL}}{Z_2^{CL^2}}. \quad \text{(A11)}$$

Consequently, $\frac{c}{R_2^{NCL}}\left(R_2^{NCL}\mathrm{CP}_3 - x_2^2\right)$ is a bounded function for $x_2 \in [-1,1]$ and the value of $\frac{c}{R_2^{NCL}}\left(R_2^{NCL}\mathrm{CP}_3 - x_2^2\right)$ at $x_2 = \pm1$ are the same. Furthermore, $\frac{c}{R_2^{NCL}}\left(R_2^{NCL}\mathrm{CP}_3 - x_2^2\right)$ is a concave function for $x_2 \in [-1,1]$. As proved previously, $(\mathrm{CP}_1 - x_2^2)^2 + (\mathrm{CP}_2 + \sqrt{(1-x_2^2)}x_2)^2$ is also a bounded function and only have one maximal and one minimal value for $x_2 \in [-1,1]$. The value of $(\mathrm{CP}_1 - x_2^2)^2 + (\mathrm{CP}_2 + \sqrt{(1-x_2^2)}x_2)^2$ at $x_2 = \pm1$ are also the same. In this way, the curve between P_2^D and x_2 only has one maximal value and one minimal value as shown in Fig. 9(b) as an example. Finally, owing to both of P_2^D and V_2 achieve the maximal and minimal value only once for $x_2 \in [-1,1]$ and both the value of them

This article has been accepted for publication in a future issue of this journal, but has not been fully edited. Content may change prior to final publication. Citation information: DOI 10.1109/TSG.2016.2609603, IEEE Transactions on Smart Grid

keep the same at $x_2 = \pm 1$. In this way, a closed curve similar to an ellipse can be obtained for the operating trace of an ES with a resistive NCL as shown in Fig. 9(c) as an example.

C. Derivation of Calculations

Let $\frac{d\gamma}{dx} = 0$, x_k can be solved as follows,

$$\sin\varphi_k^{NCL} - \frac{x_k \cos^2\varphi_k^{NCL}}{\sqrt{1-\cos^2\varphi_k^{NCL} {x_k}^2}} = 0 \quad \text{(A12)}$$

$$x_k = \tan\varphi_k^{NCL}. \quad \text{(A13)}$$

Owing to $\frac{d^2\gamma_k}{d{x_k}^2} < 0$ as shown in (12), it can be concluded that when $x_k = \tan\varphi_k^{NCL}$, the γ_k can achieve the maximum value, which equals to $1/\cos\varphi_k^{NCL}$. Consequently, (13) and (14) can be obtained. Meanwhile, the minimum value of γ_k should be achieved at either of the upper limit or the lower limit of the feasible operating region of x_k, which equal to 1 and $\frac{1}{\cos\varphi_k^{NCL}}$ for an inductive NCL and $\frac{1}{\cos\varphi_k^{NCL}}$ and -1 for a capacitive NCL. For an inductive NCL, $\gamma_k = -tan\varphi_k^{NCL}$ when $x_k = -\frac{1}{\cos\varphi_k^{NCL}}$, while $\gamma_k = 0$ when $x_k = 1$. For a capacitive NCL, $\gamma_k = tan\varphi_k^{NCL}$ when $x_k = \frac{1}{\cos\varphi_k^{NCL}}$, while $\gamma_k = 0$ when $x_k = -1$. For a resistive NCL, $\gamma_k = 0$ for both $x_k = \pm 1$. Consequently, when $x_k = 1$, the minimum value of $\gamma_k = 0$ can be obtained for an inductive NCL while when $x_k = -1$, the minimum value of $\gamma_k = 0$ can be obtained for a capacitive NCL. For a resistive load, when $x_k = \pm 1$, the minimum value of $\gamma_k = 0$ can be obtained. Equation (15) can be derived as a result.

For a strong bus, the initial operating point of ES is set to make the consumed active power of the NCL equals to half of the summation of the minimum and maximum value of P_k^{NCL}, which equals to $\frac{{V_k}^2 R_k^{NCL}}{2\times {Z_k^{NCL}}^2 \cos^2\varphi_k^{NCL}}$. Consequently, the initial operating point of x_k can be calculated as $\frac{\tan\varphi_{NCL} \pm 1}{\sqrt{2}}$. Equation (18) can be obtained as a result.

For a weak bus, the initial operating point of ES is also set to make the consumed active power of the NCL equals to half of the summation of the minimum and maximum value of P_k^{NCL}, which equals to $\frac{1}{2}(\tan^2\varphi_k^{NCL} + \frac{1}{\cos^2\varphi_k^{NCL}})\frac{{V_k}^2 R_k^{NCL}}{{Z_k^{NCL}}^2}$. Consequently, the initial operating point of x_k can be calculated as $\frac{\tan\varphi_{NCL}\sqrt{1+\sin^2\varphi_k^{NCL}} \mp \cos\varphi_k^{NCL}}{\sqrt{2}}$. Equation (18) can be obtained as a result.

Liang Liang (S'13) received the B.E. degree in electrical engineering from Tsinghua University, Beijing, China, in 2005, and M.S. degree from the Institute of Electrical Engineering, Chinese Academy of Sciences, Beijing China, in 2008.

He was an engineer at Siemens Ltd., China and China Electric Power Research Institute. He is currently pursuing the Ph.D degree in electrical and electronic engineering at the University of Hong Kong, Hong Kong, China.

His research interests include power system resilience, power system flexibility, and renewable energy integration.

Yunhe Hou (M'08-SM'15) received the B.E. and Ph.D. degrees in electrical engineering from the Huazhong University of Science and Technology, Wuhan, China, in 1999 and 2005, respectively.

He was a Post-Doctoral Research Fellow at Tsinghua University, Beijing, China, from 2005 to 2007, and a Post-Doctoral Researcher at Iowa State University, Ames, IA, USA, and the University College Dublin, Dublin, Ireland, from 2008 to 2009. He was also a Visiting Scientist at the Laboratory for Information and Decision Systems, Massachusetts Institute of Technology, Cambridge, MA, USA, in 2010. He joined the faculty of the University of Hong Kong, Hong Kong, in 2009, where he is currently an Assistant Professor with the Department of Electrical and Electronic Engineering.

Dr. Hou is an Editor of the IEEE TRANSACTIONS ON SMART GRID and an Associate Editor of JOURNAL OF MODERN POWER SYSTEMS AND CLEAN ENERGY.

David J. Hill (S'72-M'76-SM'91-F'93-LF'14) received the PhD degree in Electrical Engineering from the University of Newcastle, Australia, in 1976. He holds the Chair of Electrical Engineering in the Department of Electrical and Electronic Engineering at the University of Hong Kong. He is also a part-time Professor of Electrical Engineering at The University of Sydney, Australia.

During 2005-2010, he was an Australian Research Council Federation Fellow at the Australian National University. Since 1994, he has held various positions at the University of Sydney, Australia, including the Chair of Electrical Engineering until 2002 and again during 2010-2013 along with an ARC Professorial Fellowship. He has also held academic and substantial visiting positions at the universities of Melbourne, California (Berkeley), Newcastle (Australia), Lund (Sweden), Munich and in Hong Kong (City and Polytechnic).

His general research interests are in control systems, complex networks, power systems and stability analysis. His work is now mainly on control and planning of future energy networks and basic stability and control questions for dynamic networks.

Professor Hill is a Fellow of the Society for Industrial and Applied Mathematics, USA, the Australian Academy of Science and the Australian Academy of Technological Sciences and Engineering. He is also a Foreign Member of the Royal Swedish Academy of Engineering Sciences.

S. Y. (Ron) Hui (M'87–SM'94–F'03) received the B.Sc. (Eng.) degree from the University of Birmingham, Birmingham, U.K., in 1984, and the D.I.C. and Ph.D. degrees from Imperial College London, London, U.K., in 1987.

He currently holds the Philip Wong Wilson Wong Chair Professorship at the University of Hong Kong, Hong Kong, and a Part-Time Chair Professorship at Imperial College London. He has published more than 300 technical papers, including more than 190 refereed journal publications. More than 55 of his patents have been adopted by industry. He is an Associate Editor of the IEEE TRANSACTIONS ON POWER ELECTRONICS and IEEE TRANSACTIONS ON INDUSTRIAL ELECTRONICS, and an Editor of the IEEE JOURNAL OF EMERGING AND SELECTED TOPICS IN POWER ELECTRONICS. His inventions on wireless charging platform technology underpin key dimensions of Qi, the world's first wireless power standard, with freedom of positioning and localized charging features for wireless charging of consumer electronics.

Prof. Hui, in November 2010, received the IEEE Rudolf Chope R&D Award from the IEEE Industrial Electronics Society and the IET Achievement Medal (The Crompton Medal). He is a Fellow of the Australian Academy of Technological Sciences and Engineering and is the recipient of the 2015 IEEE William E. Newell Power Electronics Award. He is an Academician of Royal Academy of Engineering, U.K.